J. Electrochem. Sci. Eng. **14(5)** (2024) 535-546; http://dx.doi.org/10.5599/jese.2449

Open Access : : ISSN 1847-9286
https://pub.iapchem.org/ojs/index.php/JESE

Original scientific paper

High-performance supercapacitor electrodes for energy storage using activated carbons from argan husks, date seeds and olive stones

Mohamed Ennabely[1,✉], Youssef Lghazi[1], Abdessamad Ouedrhiri[1], Redouane El adnani[1], Aziz Aynaou[1], Boubaker Youbi[1,2] and Itto Bimaghra[1]

[1]*Laboratoire Bio-Géosciences et Ingénierie des Matériaux. Ecole Normale Supérieure. Université Hassan II de Casablanca, 50069, Morocco*

[2]*Centre Régional des Métiers de l'Education et de la Formation Casablanca-Settat. Casablanca, Morocco*

Corresponding authors: ✉ennabely.mohamed@gmail.com; Tel: 0622228181

Received: August 3, 2024; Accepted: September 14, 2024; Published: September 19, 2024

Abstract

Electrochemical performances of three electrodes (E) fabricated using activated carbons (AC) derived from agricultural biomass waste, specifically argan husks (ah), date seeds (ds) and olive stones (os), denoted ACah-E, ACds-E and ACos-E respectively were evaluated. These activated carbons were produced through a combination of thermal and chemical methods, involving carbonization for 2 hours at a temperature of 900 °C, followed by chemical activation using phosphoric acid as the activating agent. The scanning electron microscope observations revealed that the obtained samples exhibited variable pore size distributions tailored based on the raw materials activated by the same process. Subsequently, cyclic voltammetry, galvanostatic charge-discharge, and electro-chemical impedance spectroscopy were used to characterize the electrochemical performances of ACah-E, ACds-E and ACos-E as supercapacitor electrodes. The results revealed that the ACah-E, ACds-E and ACos-E cells have specific capacitances of 138.26, 50.41 and 34.61 F/g, respectively. These results were found to be influenced by the specific surface areas, which were 476 m²/g for ACah, 441 m²/g for ACds and 362 m²/g for ACos, as determined by the BET method. The behaviour of electrochemical double-layer capacitors (EDLC) in acidic aqueous electrolyte (1 M H_2SO_4) is demonstrated by these findings, which suggest that the waste materials used may also be prospective candidates for supercapacitor applications, with the best performance for ACah-E than other.

Keywords

Activated carbons; agricultural waste; capacitive electrodes; gravimetric capacitance; energy storage

Introduction

The growing energy demand necessitates innovative solutions that offer high performance, affordability, and minimal environmental impact. The principal aim of new research studies delves into the creation of sustainable generation energy storage and production systems with these characteristics. The development of high-performing supercapacitors, batteries, and fuel cells is a major area of research focus. Within this field, a critical objective lies in identifying and designing novel materials that are both environmentally friendly and cost-effective for the efficient utilization of these devices. In this context, the use of solid waste for depollution and energy storage presents a particularly innovative solution, especially when employing biomass-derived activated carbon.

Morocco generates a significant amount of agricultural waste, particularly argan husks [1], dates seeds [2] and olive stones [3]. Indeed, the production has increased to 4,000 tons due to the growing demand for argan oil worldwide for food and other applications, but this still leaves behind 80,000 tons of wasted waste [4], which is equal to or more than the amount of waste from dates and olives. Although these by-products are not economically valuable or of immediate use, they can be very promising in the development of activated carbon-based porous electrodes for supercapacitors. Utilizing these materials for energy storage through supercapacitor electrodes, recycling this waste to produce activated carbon appears to be a solution to reduce environmental pollution [5].

Biomass-derived activated carbons have recently been utilized as electrode materials in electrochemical capacitors owing to their exceptional features, such as a unique internal structure, consistently interconnected mesopores, high specific surface area, low mass density, impressive chemical stability, reasonable cost, and eco-friendliness. These attributes make them highly promising for use as electrodes [6]. When a solid comes into contact with a saline solution, it forms a charge distribution at the interface, creating a capacitor with reduced capacity. However, in the case of activated carbon, its high specific surface area enables the creation of supercapacitors suitable for systems requiring large-scale energy storage and distribution [7]. For instance, Elmouwahidi *et al.* succeeded in obtaining supercapacitor electrodes using activated carbons from argan nuts, with a specific surface area of 2100 m^2/g and a specific capacitance of ∼329 F/g at a current density of 1 A/g, in an aqueous electrolyte (1M H_2SO_4) [8].

In this work, we have successfully utilized activated carbons from three sources: argan husks (ah), date seeds (ds) and olive stones (os) to develop three electrodes (E) denoted ACah-E, ACds-E, and ACos-E for supercapacitor applications. We evaluated the enhancement of their surface area and the development of tailored porosity through selective chemical activation with phosphoric acid applied to the initial carbonized material. Subsequently, three electrodes will be fabricated, and their electrochemical performances will be examined by using cyclic voltammetry, galvanostatic charge-discharge, and electrochemical impedance spectroscopy.

Experimental

Activation process for materials production

The biomass waste materials, namely argan husks, were collected from the Moroccan South Atlantic, while date seeds and olive stones were collected from regions of Settat, Morocco. They were cleansed using distilled water to eliminate impurities and then dried at 120 °C for 12 hours in an oven. The resulting products were ground and sieved using a 5 μm pore sieve to obtain untreated raw materials in powder form. Next, the carbonization step took place in a furnace (PROTERM-PLF 120/6) at 900 °C for two hours.

The chemical activation process of the obtained powder was carried out by adding phosphoric acid at a weight ratio of 1:2. Distilled water was then added to the mixture, reaching a volume of 50 ml, and the mixture was stirred for 10 minutes. The samples were left to dry overnight at 120 °C and subsequently washed with demineralized water and sodium hydroxide until neutralization was achieved to eliminate any remaining residual amounts of H_3PO_4 [9]. Finally, the activated carbons ACah, ACds and ACos were filtered, dried at 120 °C for 12 hours, and stored in small glass jars, as shown in Figure 1.

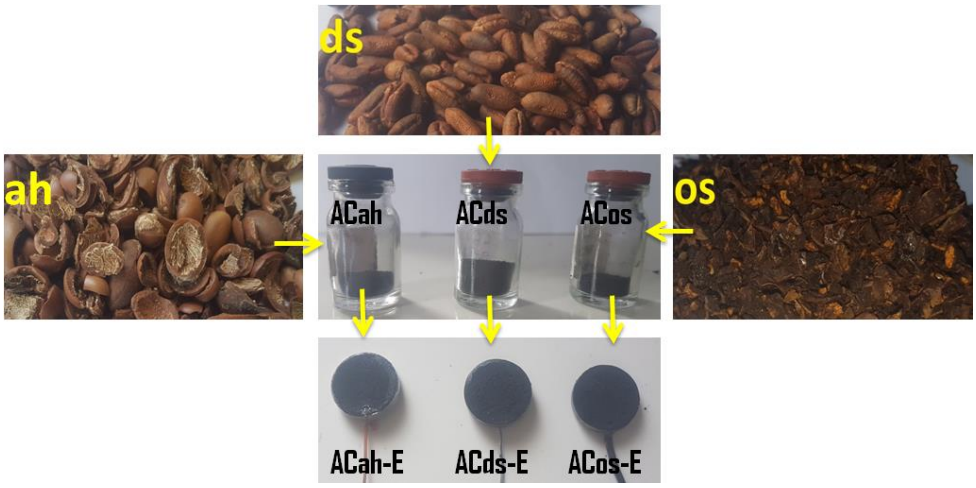

Figure 1. *Three precursors, their activated carbons and prepared electrodes*

Characterization of activated carbons

The FTIR analysis was carried out using a TENSOR 27 type spectrometer (Bruker Company, Germany) for three samples obtained by mixing 100 mg of potassium bromide with 1 mg of each activated carbon, the data was recorded in the 4000-500 cm^{-1} range to plot IR spectra. Scanning electron microscopy (SEM) of three activated carbons has been performed using a Philips XL 30FEG with a secondary electron detector (SE) and an electron acceleration voltage of 20 kV. Also, our activated carbons-BET surface area was ascertained by N_2 adsorption-desorption measurements using an automated Micromeritics system running at 77 K [10].

Preparation of electrodes

The activated carbon working electrodes were fabricated by combining 85 % activated carbon, 10 % carbon black for conductivity, and 5 % polytetrafluoroethylene (PTFE) as a binding agent. After grinding, the mixture was pressed onto a stainless-steel mesh current collector with a surface area of 2.5 cm^2 having 4 mg as the mass of active electrode material. The electrodes were then dried for 8 hours at 100 °C.

Electrochemical measurements

The electrochemical performances of the activated carbon electrodes ACah-E, ACds-E and ACos-E were measured in a cell using (1 M H_2SO_4) as the electrolyte. Electrochemical characterization, employing cyclic voltammetry (CV), galvanostatic charge-discharge (GCD), and electrochemical impedance spectroscopy (EIS), was also performed to evaluate their performance. Indeed, the electrochemical performance of the prepared activated carbon electrodes was evaluated at room temperature using a computer-controlled Versa Stat 3 potentiostat. In the electrochemical cell, three electrodes were used for each experiment: activated carbon as the working electrode, platinum as the counter electrode, and a saturated calomel electrode (SCE) as the reference. The

CV experiments were carried out in the potential range of -0.4 to 0 V, this voltage window ensures the stability of the materials of these three electrodes in the electrolyte used (1 M H_2SO_4). Beyond this range, electrochemical tests have shown a significant degradation of the material due to the evolution of gases from the solvent.

The specific capacitance was calculated from the CV curves following equation (1):

$$C_{CV} = \frac{\int i(E)\mathrm{d}E}{2mv\Delta E} \quad (1)$$

Where C_{CV} / F g^{-1} is specific (gravimetric) capacitance, m / g is the mass of the electrode material, v / V s^{-1} is the potential scan rate and ΔE / V is the voltage window.

From the GCD analysis, the specific (gravimetric) capacitance C_{GCD} / F g^{-1} of the electrodes can be calculated using equation (2) [11]:

$$C_{GCD} = \frac{I\Delta t}{m\Delta E} \quad (2)$$

In equation (2), I/A is the discharge current, Δt/s represents discharge time, m/g is the effective mass loaded on a single working electrode, and ΔE/V is the potential window of discharge [12].

Results and discussion

Physicochemical characterizations of activated carbons

FTIR-analysis

The physical and chemical properties of the materials utilized are crucial in understanding electrochemical behaviours. Fourier transform infrared spectroscopy is one of the most important tools for this purpose because it allows for a qualitative examination of the surface functional groups [13] of ACah, ACds, and ACos. Figure 2 displays the FTIR spectra of the three adsorbents.

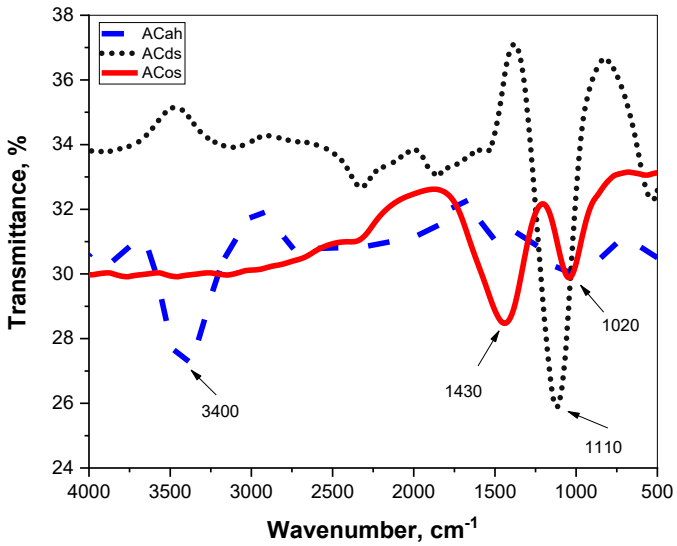

***Figure 2**. FTIR-spectra of ACah, ACds and ACos*

These spectra reveal unique properties for each material:

- Due to the stretching vibration of the hydroxyl groups produced by the O-H bond, ACah exhibits a distinct and broad band at about 3400 cm^{-1} [14].
- ACds exhibits a peak around 1110 cm^{-1}, which corresponds to the presence of C-O groups in secondary alcohol groups [15].

- ACos shows a distinct peak at approximately 1430 cm^{-1}, indicating C-H vibrations within the methylene linkage[16]. Additionally, there are peaks at 1020 cm^{-1}, signifying C-O vibrations related to oxygen-containing groups [17].

SEM-analysis

The SEM images presented in Figure 3 reveal the structural and morphological characteristics of ACah, ACds, and ACos.

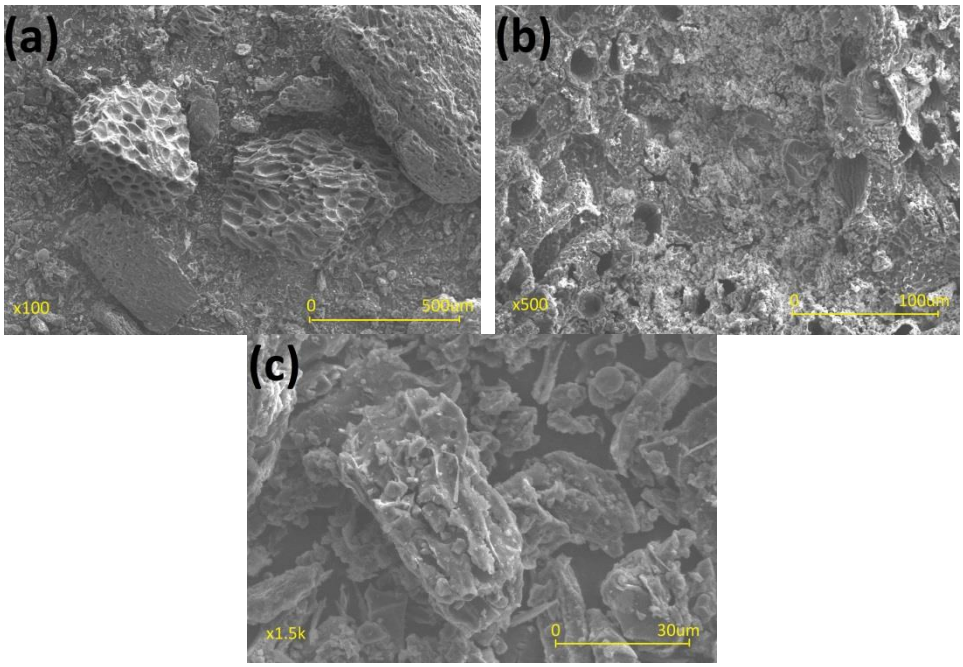

***Figure 3**. SEM-images of ACah (a), ACds (b), and ACos (c)*

It is clear that the rough texture of the ACah surface, which has many small-diameter pores, makes it unique. This promotes the molecules penetration into the material and raises the possibility of energy storage [18], Whereas ACos has a rough surface with thin films and granules that can improve the attraction of molecules on the electrode surface [19], ACds has an uneven surface structure with micropores. The specific surface areas of our adsorbents are also calculated using the BET analysis method. The BET-specific surface area of 476, 441, and 362 m^2 g^{-1} are obtained respectively for ACah, ACds and ACos materials. Compared to the other two adsorbents under study, ACah has a noticeably larger specific surface area. The quantitative interpretation of the BET surface area agrees with the results, as shown in Figure 3, indicating that ACah has a higher value compared to the others. This is due to its porous structure, as revealed by the SEM analysis, which enhances energy storage. Therefore, argan shells can play a significant role in the development of more efficient double-layer electrodes.

Electrochemical performances

Cyclic voltammetry

Cyclic voltammetry is a useful method for determining the capacitive behaviour of the material used as the supercapacitor electrode. This method was used to evaluate the capacitance of the newly developed electrode materials (ACah, ACds, and ACos). Figure 4 displays the CV curves obtained after each electrode was assessed separately in a 1M H_2SO_4 electrolyte solution using a voltage window from -0.4 to 0 V at different potential scan rates between 1 and 4 mV/s.

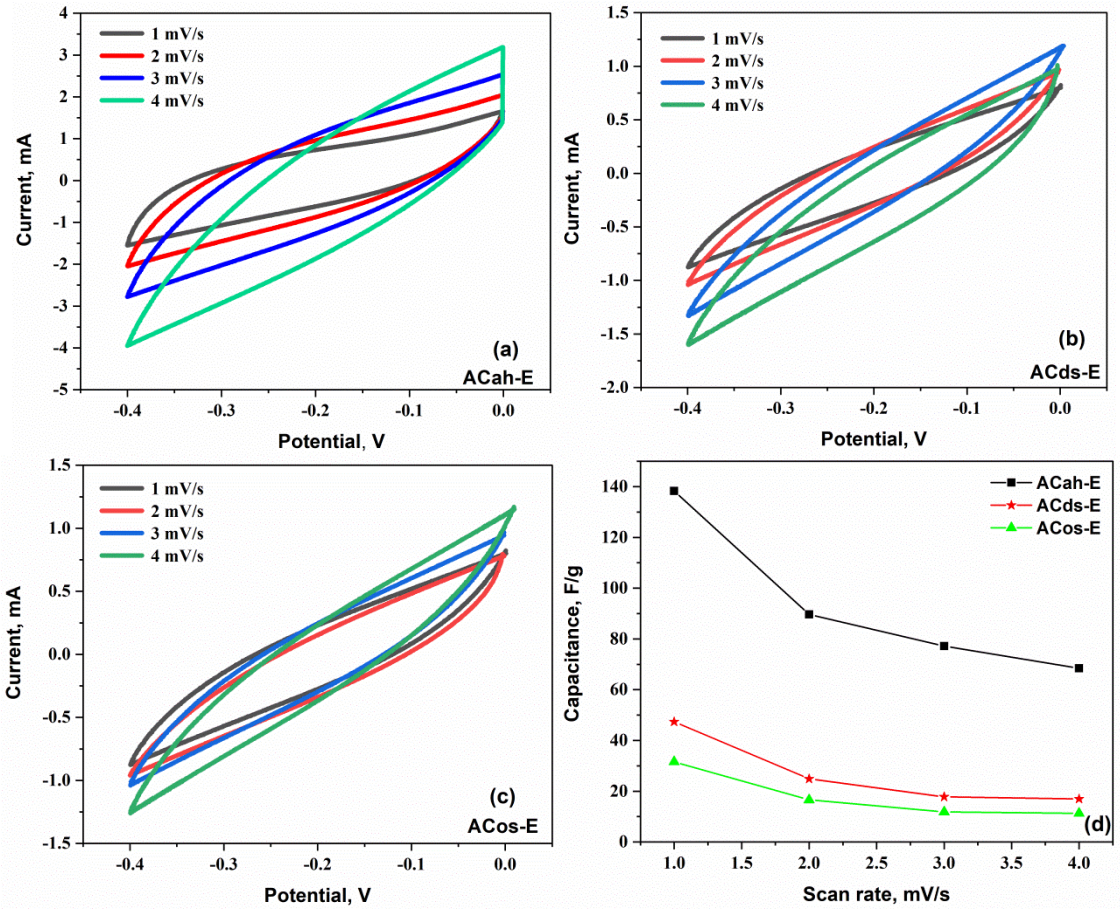

Figure 4. *Cyclic voltammograms at different potential scan rates of ACah-E (a), ACds-E (b), ACos-E (c) in 1M H_2SO_4 electrolyte, and gravimetric capacitance vs. scan rate (d)*

Cyclic voltammetry (CV) traces for the fabricated ACah-E, ACds-E, and ACos-E electrodes show quasi-rectangular curves at different potential scan rates, demonstrating the general dominance of electrochemical double-layer capacitor (EDLC) behaviour.

One essential feature of a capacitive electrode is that its response is highly dependent on the sweep rate at which cyclic voltammetry is carried out. Figure 4 shows no evidence of redox current in the voltammetric sweeps, and the current is nearly constant throughout most of the potential range. The CV curves gradually slope with increasing scan speed, maintaining their rectangular shape and growing cycle area. This clearly indicates that the studied electrodes have capacitive characteristics when used with aqueous 1M H_2SO_4 solution.

The ACah-E sample in Figure 4(a) has the largest surface area of CV loops of all the samples due to porous surface interaction of ionic adsorption and insertion favoured by the availability of functional groups, as shown in FTIR spectra in Figure 2 [19]. However, the ACos-E sample in Figure 4(c) shows smaller loop areas compared to the other samples at the same potential scan speed. The earlier mentioned BET values suggest that the observed difference is probably related to the proportion of micropores and the reduced specific surface area in this sample.

The specific gravimetric capacitance values of ACah-E, ACds-E, and ACos-E are plotted as a function of the potential scan rate in Figure 4(d). According to equation (1), the specific capacitance decreases for all samples as the scan rate increases due to the diffusion limitations of electrolyte ions within the pores of the material [20]. The ACah-E sample exhibits superior capacitive performance, with the highest specific capacitance values of 138.26 F/g at the scan rate of 1 mV/s and 68.43 F/g at 4 mV/s. This can be attributed to its highest specific surface area. In contrast, the

ACds-E and ACos-E samples show relatively low and similar specific capacitance values despite having nearly identical surface areas. The ACos-E sample, in particular, demonstrates the lowest capacitance values of 31.06 F/g at a scan rate of 1 mV/s and 11.16 F/g at 4 mV/s, which is attributed to its lower surface area and the smallest number of pores.

Galvanostatic charge-discharge (GCD)

The GCD test was performed in the -0.4 to 0 V potential window at a current ranging from 2 to 8 mA (0.5 to 2 A/g) to verify the electrochemical performance of the three electrodes and the results are shown in Figure 5.

The GCD curves for ACah-E, ACds-E, and ACos-E all show a near-perfect triangular shape with minimal initial voltage drop. This initial jump (sudden rise in potential) might be due to the inherent resistance of the electrodes. The key takeaway is the triangular shape, which is a hallmark of ideal supercapacitor behavior (EDLC). Even at high currents, all three materials maintain this triangular profile, indicating efficient transfer of ions within the electrodes. However, the emergence of curvature in the curves at lower currents indicates surface faradaic reactions attributed to pseudocapacitance behavior [21]. It can, therefore, be concluded that our prepared electrodes are suitable for capacitive applications and have good charge-discharge density values.

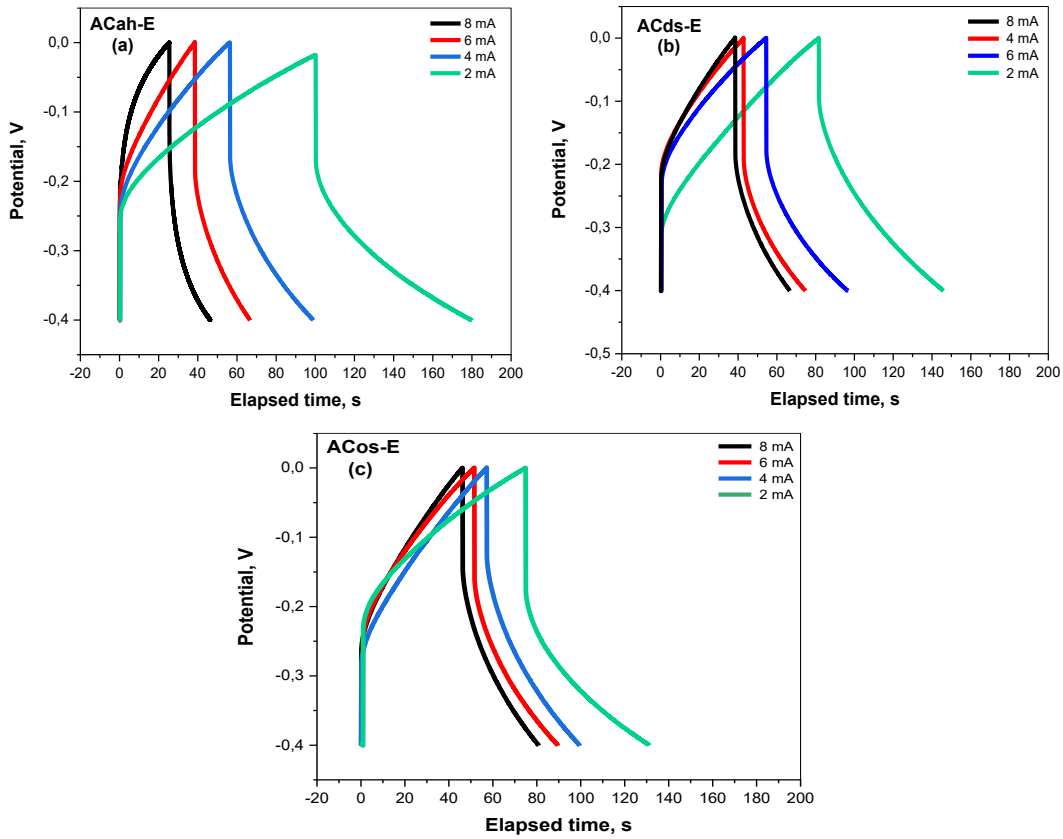

Figure 5. *Charge discharge curves of ACah-E(a); ACds-E(b) and ACos-E(c)*

The resistance, *R*, represents various resistive parameters of an electrode system, including solution resistance, electron transfer resistance across the electrode-electrolyte interface [22], resistance to ion diffusion within the electrode, *etc*. Resistance *R* was calculated from the curves using equation (3), where Δ*E* / V is the voltage window and *I* / A is the applied current and, illustrated in Figure 6.

$$R = \frac{\Delta E}{I} \qquad (3)$$

As shown in Figure 5, a sharp drop in initial voltage during discharge is evident and results probably from the diffusion-limited mobility of electrolyte ions in the electrode pores. This limitation decreases as a function of current intensity, as shown in Figure 6. The resistance (*R*) values of ACas-E, ACds-E and ACos-E are 20, 21 and 26 Ohm, respectively, clearly indicating that the ACah-E offers the lowest *R* value at 8 mA.

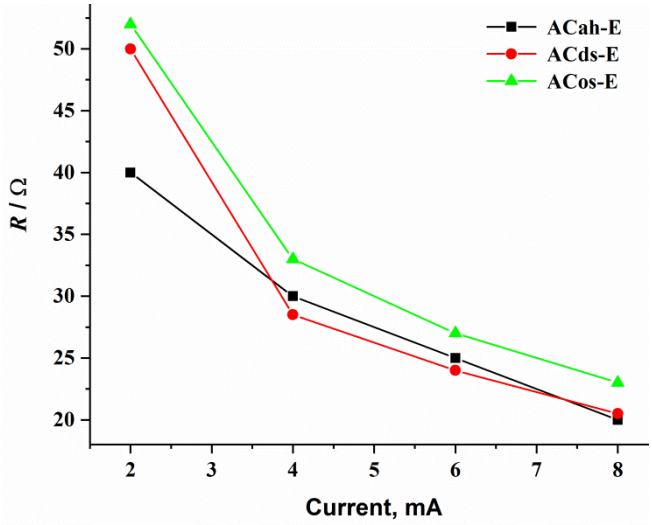

Figure 6. *Resistance R as a function of current intensity*

From the chronopotentiograms shown in Figure 5 at a current load of 2 mA (0.5 A/g), the values of specific (gravimetric) capacitance (*Cs*) were calculated using equation (2) and are compiled in Table 1.

Table 1. *Specific (gravimetric) capacitance values for ACah-E, ACds-E, and ACos-E*

	ACah-E	ACds-E	ACos-E
C_s / F g^{-1}	100.41	81.61	72.13

The results presented in Table 1, in conjunction with previous findings, suggest that waste products such as argan, date, and olive residues are promising materials for supercapacitor applications. When used in an acidic aqueous electrolyte (1 M H_2SO_4), these materials exhibit the characteristics of electrochemical double layer capacitors (EDLCs), with argan material demonstrating the best performance.

The findings, along with previous results, suggest that argan waste shows promise as a material for supercapacitor applications. It exhibits the characteristics of electrochemical double-layer capacitors (EDLC) when used in an acidic aqueous electrolyte (1 M H_2SO_4).

Electrochemical impedance

Electrochemical impedance spectroscopy measurements were performed at the open circuit potential by imposing a 5 mV sinusoidal perturbation over the 100 kHz to 10 mHz frequency range on three electrodes, each with a surface area of 2.5 cm^2. A simple electrochemical impedance model was discussed according to the Nyquist diagram obtained. To find different parameters related to the working electrode under study, the experimental results were fitted to this theoretical model.

The Nyquist impedance plots of the cell are shown in Figure 7. All electrodes displayed typical AC impedance characteristics of supercapacitors. A semicircle was observed at high frequencies, followed by a sloping line in the low-frequency region representing the Warburg impedance associated with diffusion-limited processes (diffusion of ions within the electrode pores toward electrode/solution interphase).

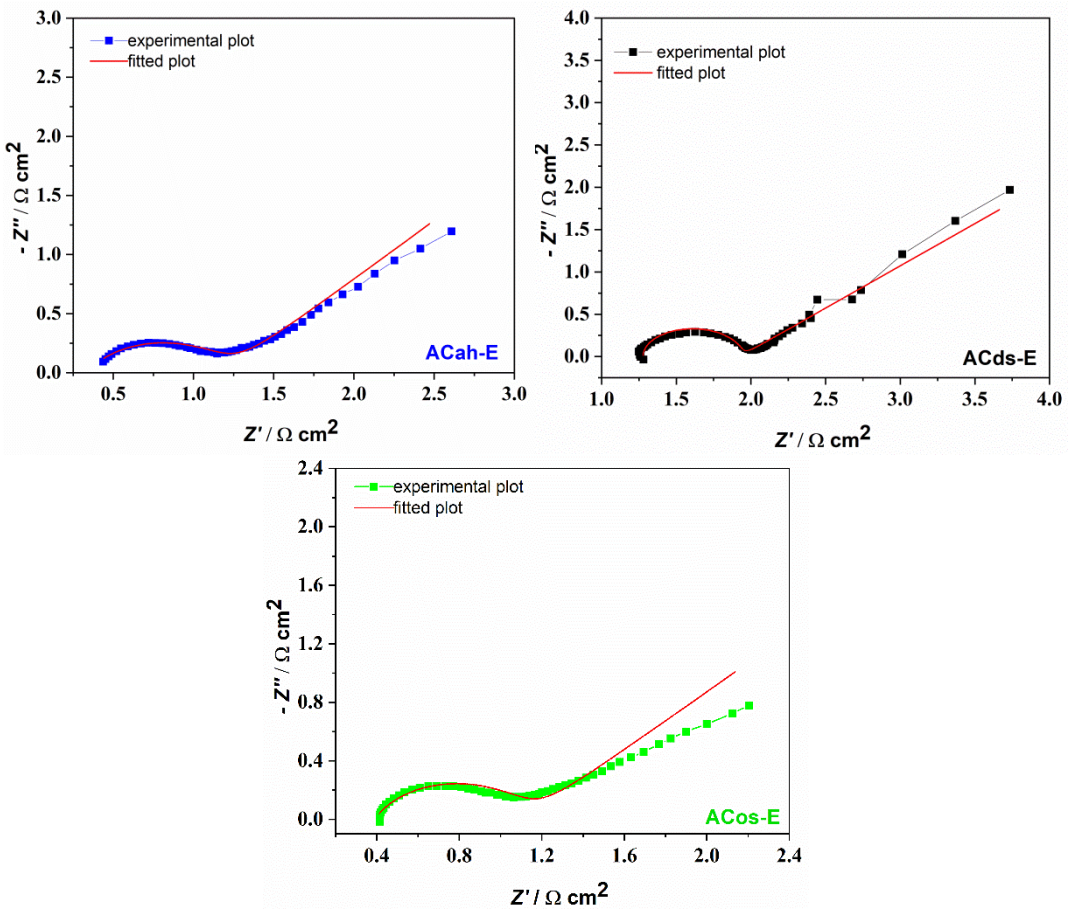

Figure 7. *Experimental and fitted impedance plots of ACah-E, ACds-E, and ACos-E*

Different resistive and capacitive contributions in electrochemical systems are generally described by equivalent circuit models used in electrochemical impedance spectroscopy (EIS)[23]. These models can vary depending on the specific configuration of the electrochemical cell and the processes taking place within it.

To describe the impedance of the electrochemical cell using the ZSIM DEMO program [24], an equivalent circuit is shown in Figure 8. This circuit consists of an uncompensated electrolyte resistance term with possible contributions of the bulk electrode and contact resistances (R_b) in series with a parallel combination of a charge transfer and/or bulk solution resistance within pores of electrode material (R_{ct}) and ideal capacitor due to the double layer denoted as C_{dl} [25]. The diffusion impedance, associated with the movement of reactive species toward the electrode interface within pores, is represented by the Warburg element (W) [26]. This element is characterized by a linear response with approximately -45° slope angle, which emerges immediately after the semicircle on the x-axis, as illustrated in Figure 7.

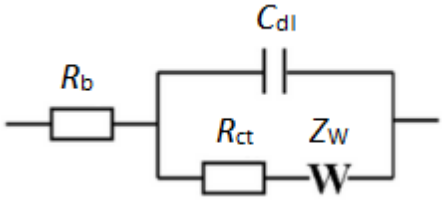

Figure 8. *Equivalent electrical circuit adjusted to experimental impedance results of ACah-E, ACds-E and ACos-E*

In the Nyquist diagram of each electrode, the semicircle intercepts on the x-axis at higher frequencies correspond to R_b and R_b+R_{ct}, respectively. The linear part at lower frequencies describes

the Warburg region, where the diffusion process of electrolyte ions into pores of electrode material is a dominating process. These parameters are defined by model equation (4) and were determined using the ZSIM DEMO program; they are subsequently listed in Table 2.

$$Z = R_b + \frac{R_{ct} + Z_W}{1 + j\omega\left(R_{ct} + Z_W\right)C_{dl}} \quad (4)$$

where Z is the impedance of the electrochemical system, Z_W represents the Warburg impedance, j is the imaginary unit and ω is the angular frequency ($\omega=2\pi f$, where f is the frequency).

***Table 2**. Impedance parameter values for ACah-E, ACds-E and ACos-E obtained by fitting EEC in Figure 8 to impedance spectra in Figure 7*

Electrode	R_b / Ω cm^2	R_{ct} / Ω cm^2	C_{dl} / mF cm^{-2}	W / S s$^{0.5}$ cm^{-2}
ACah-E	0.442	0.804	0.1540	0.2723
ACds-E	1.279	0.696	0.1233	0.2692
ACos-E	0.417	0.738	0.0949	0.2302

In the high-frequency region, the diameter of the semicircle is significantly small, which is usually a measure of charge transfer resistance (R_{ct}) [27]. The obtained values in Table 2 confirm the pseudocapacitive behaviour concluded from the CV and CGD analyses. Specifically, the Warburg element and the resistances R_b and R_{ct} are low, reflecting reduced charge transfer resistance and diminished diffusion effects. Furthermore, in the medium and low frequencies range, the impedance spectrum clearly reflects a linear behaviour with a slope of about -45° showing electrolyte ion diffusion for double-layer formation within pores of electrode material [28], with ACah-E having a higher double-layer capacitance C_{dl} than the other electrodes ACds-E and ACos-E.

Conclusion

The preparation and characterization of three high-performance electrodes, designated as ACah-E, ACds-E, and ACos-E, utilized inexpensive activated carbon derived from agricultural waste: argan husks, date seeds, and olive stones. The activation process used H_3PO_4 as the activating agent. It was confirmed that argan-based activated carbon (ACah-E) has more developed porosity and a larger BET surface area compared to the activated carbon from date seeds (ACds-E) and olive stones (ACos-E), respectively. The surface morphology and porosity of the activated carbons were revealed, with ACah-E showing a more developed structure. The capacitive behaviour of all three electrodes was demonstrated, with ACah-E electrode exhibiting a significantly higher specific capacitance than ACds-E and ACos-E. Argan waste, due to its distinctive characteristics, ease of preparation, and abundant availability, is considered a viable renewable energy source. This waste material shows great potential for application in supercapacitors, particularly as an electrochemical double-layer capacitor (EDLC). Overall, the study highlights the potential of argan-based activated carbon for high-performance electrode applications in renewable energy technologies.

References

[1] F. Z. Zouhair, A. Benali, M. R. Kabbour, K. EL Kabous, E. haj El Maadoudi, M. Bouksaim, A. Essamri, Typical characterization of argane pulp of various Moroccan areas: A new biomass for the second generation bioethanol production, *Journal of the Saudi Society of Agricultural Sciences* **19** (2020) 192-198. https://doi.org/10.1016/j.jssas.2018.09.004

[2] O. Kerrou, N. Lahboubi, M. Bakraoui, F. Karouach, Y.E. Gnaoui, A. Schüch, W. Stinner, H.E. Bari, Methane production from anaerobic digestion of date palm leaflet waste in Morocco, *Journal*

of Material Cycles and Waste Management **23** (2021) 15991608. https://doi.org/10.1007/s10163-021-01238-z

[3] I. Alaoui, O. El Ghadraoui, K. Tanji, A. Harrach, A. Farah, The Olive Mill Pomace: A Sustainable Biofertilizer to Improve Soil Proprieties and Plant Nutrient Uptake, *Waste and Biomass Valorization* **15** (2024) 2575-2590. https://doi.org/10.1007/s12649-023-02324-z

[4] H. El Ouahabi, A. Elmouwahidi, L. Cano-Casanova, M. Á. Lillo-Ródenas, M. C. Roman-Martínez, A.F. Pérez-Cadenas, E. Bailón-García, M. Shaban, G.M. Al-Senani, M. Ouzzine, M. Khaddor, From nutshells to energy cells: Pioneering supercapacitor electrodes via innovative argan nutshell activated carbon synthesis, *Journal of Energy Storage* **82** (2024) 110598. https://doi.org/10.1016/j.est.2024.110598

[5] M. Maharjan, Conversion of carbon based food wastes to electrodes for energy storage applications, Doctoral Thesis, Nanyang Technological University, Singapore, 2018. https://doi.org/10.32657/10356/74868

[6] A. A. Mohammed, C. Chen, Z. Zhu, Low-cost, high-performance supercapacitor based on activated carbon electrode materials derived from baobab fruit shells, *Journal of Colloid and Interface Science* **538** (2019) 308-319. https://doi.org/10.1016/j.jcis.2018.11.103

[7] M. Bora, D. Bhattacharjya, B. K. Saikia, Coal-Derived Activated Carbon for Electrochemical Energy Storage: Status on Supercapacitor, Li-Ion Battery, and Li-S Battery Applications, *Energy Fuels* **35** (2021) 18285-18307. https://doi.org/10.1021/acs.energyfuels.1c02518

[8] A. Elmouwahidi, Z. Zapata-Benabithe, F. Carrasco-Marín, C. Moreno-Castilla, Activated carbons from KOH-activation of argan (*Argania spinosa*) seed shells as supercapacitor electrodes, *Bioresource Technology* **111** (2012) 185-190. https://doi.org/10.1016/j.biortech.2012.02.010

[9] Y. Li, X. Zhang, R. Yang, G. Li, C. Hu, The role of H_3PO_4 in the preparation of activated carbon from NaOH-treated rice husk residue, *RSC Advances* **5** (2015) 32626-32636. https://doi.org/10.1039/C5RA04634C

[10] F. Koyuncu, F. Güzel, İ. I. G. İnal, High surface area and supermicroporous activated carbon from capsicum (*Capsicum annuum* L.) industrial processing pulp via single-step KOH-catalyzed pyrolysis: Production optimization, characterization and its some water pollutants removal and supercapacitor performance, *Diamond and Related Materials* **124** (2022) 108920. https://doi.org/10.1016/j.diamond.2022.108920

[11] J. Yu, N. Fu, J. Zhao, R. Liu, F. Li, Y. Du, Z. Yang, High Specific Capacitance Electrode Material for Supercapacitors Based on Resin-Derived Nitrogen-Doped Porous Carbons, *ACS Omega* **4** (2019) 15904-15911. https://doi.org/10.1021/acsomega.9b01916

[12] O. Boujibar, A. Ghosh, O. Achak, T. Chafik, F. Ghamouss, A high energy storage supercapacitor based on nanoporous activated carbon electrode made from Argan shells with excellent ion transport in aqueous and non-aqueous electrolytes, *Journal of Energy Storage* **26** (2019) 100958. https://doi.org/10.1016/j.est.2019.100958

[13] P. Azhagapillai, A. Al Shoaibi, S. Chandrasekar, Surface functionalization methodologies on activated carbons and their benzene adsorption, *Carbon Letters* **31** (2021) 419-426. https://doi.org/10.1007/s42823-020-00170-w

[14] G. L. Arueya, T. M. Oyewale, Effect of varying degrees of succinylation on the functional and morphological properties of starch from acha (Digitaria exilis Kippis Stapf), *Food Chemistry* **177** (2015) 258-266. https://doi.org/10.1016/j.foodchem.2015.01.019

[15] B. Biswas, A. Arun Kumar, Y. Bisht, R. Singh, J. Kumar, T. Bhaskar, Effects of temperature and solvent on hydrothermal liquefaction of *Sargassum tenerrimum* algae, *Bioresource Technology* **242** (2017) 344-350. https://doi.org/10.1016/j.biortech.2017.03.045

[16] V. Arjunan, R. Anitha, L. Devi, S. Mohan, H. Yang, Comprehensive quantum chemical and spectroscopic (FTIR, FT-Raman, ^{1}H, ^{13}C NMR) investigations of (1,2-epoxyethyl)benzene and

(1,2-epoxy-2-phenyl)propane, *Spectrochimica Acta Part A: Molecular and Biomolecular Spectroscopy* **135** (2015) 120-136. https://doi.org/10.1016/j.saa.2014.07.001
[17] A. Ouedrhiri, Y. Lghazi, J. Bahar, M. Ait Himi, C. El Haimer, B. Youbi, M. Khoukhi, Y. Bimaghra, Adsorption of the Methylene Blue Dye in Environmental Water Samples by Biochar Obtained from the Valorization of Argan Shells, *Physical Chemistry Research* **10** (2022) 301-313. https://doi.org/10.22036/pcr.2021.303554.1968
[18] M. Zhang, T. Xu, D. Wang, T. Yao, Z. Xu, Q. Liu, L. Shen, Y. Yu, A 3D-Printed Proton Pseudocapacitor with Ultrahigh Mass Loading and Areal Energy Density for Fast Energy Storage at Low Temperature, *Advanced Materials* **35** (2023) 2209963. https://doi.org/10.1002/adma.202209963
[19] G. Singh, R. Bahadur, J. Mee Lee, I. Young Kim, A.M. Ruban, J.M. Davidraj, D. Semit, A. Karakoti, A.H. Al Muhtaseb, A. Vinu, Nanoporous activated biocarbons with high surface areas from alligator weed and their excellent performance for CO_2 capture at both low and high pressures, *Chemical Engineering Journal* **406** (2021) 126787. https://doi.org/10.1016/j.cej.2020.126787
[20] P. De, J. Halder, C.C. Gowda, S. Kansal, S. Priya, S. Anshu, A. Chowdhury, D. Mandal, S. Biswas, B.K. Dubey, A. Chandra, Role of porosity and diffusion coefficient in porous electrode used in supercapacitors - Correlating theoretical and experimental studies, *Electrochemical Science Advances* **3** (2023) e2100159. https://doi.org/10.1002/elsa.202100159
[21] B. Du, X. Wang, L. Chai, X. Wang, Z. Pan, X. Chen, J. Zhou, R.-C. Sun, Fabricating lignin-based carbon nanofibers as versatile supercapacitors from food wastes, *International Journal of Biological Macromolecules* **194** (2022) 632-643. https://doi.org/10.1016/j.ijbiomac.2021.11.107
[22] F. Wang, Y. Zhang, N. Yu, L. Fu, Y. Zhu, Y. Wu, T. van Ree, *Metal oxides in batteries,* in: Y. Wu (Ed.), *Metal Oxides in Energy Technologies*, Elsevier, 2018, pp. 127-167. https://doi.org/10.1016/B978-0-12-811167-3.00006-7
[23] P. I. Kyesmen, N. Nombona, M. Diale, Effects of Film Thickness and Coating Techniques on the Photoelectrochemical Behaviour of Hematite Thin Films, *Frontiers in Energy Research* **9** (2021) 683293. https://doi.org/10.3389/fenrg.2021.683293
[24] K. M. Emran, Effects of concentration and temperature on the corrosion properties of the Fe-Ni-Mn alloy in HCl solutions, *Research on Chemical Intermediates* **41** (2015) 3583-3596. https://doi.org/10.1007/s11164-013-1473-9
[25] M. Simić, A. K. Stavrakis, G. M. Stojanović, A Low-Complexity Method for Parameter Estimation of the Simplified Randles Circuit with Experimental Verification, *IEEE Sensors Journal* **21** (2021) 24209-24217. https://doi.org/10.1109/JSEN.2021.3110296
[26] P. V. Pham (ed.), *21st Century Nanostructured Materials: Physics, Chemistry, Classification, and Emerging Applications in Industry, Biomedicine, and Agriculture*, Intech. Open, 2022. http://dx.doi.org/10.5772/intechopen.94802
[27] K. Panigrahi, S. Mal, S. Bhattacharyya, Deciphering interfacial charge transfer mechanisms in electrochemical energy systems through impedance spectroscopy, *Journal of Materials Chemistry A* **12** (2024) 14334–14353. https://doi.org/10.1039/D4TA00537F
[28] T. Ahmad, M. Z. Ansari, Temperature-dependent structural and optical properties of Sb-doped SnO_2 nanoparticles and their electrochemical analysis for supercapacitor application, *New Journal of Chemistry* **48** (2024) 8495-8509. https://doi.org/10.1039/D4NJ00918E